Article

Design Considerations for Adding Series Inductors to Reduce Electromagnetic Field Interference in an Over-Coupled WPT System

Yujun Shin [1], **Jaehyoung Park** [2], **Haerim Kim** [1], **Seongho Woo** [1], **Bumjin Park** [1], **Sungryul Huh** [1], **Changmin Lee** [1] **and Seungyoung Ahn** [1,*]

[1] The Cho Chun Shik Graduate School for Green Transportation, KAIST, Daejeon 34051, Korea; yujun.shin@kaist.ac.kr (Y.S.); haerim@kaist.ac.kr (H.K.); seongho@kaist.ac.kr (S.W.); solbara@kaist.ac.kr (B.P.); tjdfuf2397@kaist.ac.kr (S.H.); ckdals4707@kaist.ac.kr (C.L.)

[2] Hardware Engineering Group, Samsung Electronics, Suwon 16677, Korea; jaebro.park@samsung.com

[*] Correspondence: sahn@kaist.ac.kr; Tel.: +82-42-350-1263

Abstract: This paper analyzes how over-coupled coils affect odd harmonic current and electromagnetic interference (EMI) in a wireless power transfer (WPT) system, and proposes design considerations for series inductors to solve the EMI problem. When the air gap of the coils of the WPT system decreases below a certain level and the coils are over-coupled, the odd harmonic component of the input impedance of the system decreases and odd harmonic currents increase. The increase in the odd harmonic components current quickly aggravates the EMI issues. To solve the EMI problem of the over-coupled WPT system, additional series inductors were applied to the system, and considerations for designing the series inductors were analyzed. When designing additional series inductors, power transfer efficiency, maximum power transfer, input impedance and odd harmonic components current must be considered. Using simulations and experiments, it was confirmed that the WPT system designed with analyzed considerations maintained relatively high efficiency and reduced EMI issues.

Keywords: wireless power transfer (WPT); over-coupled coils; electromagnetic interference (EMI) reduction; series inductors; topology; input impedance

1. Introduction

Wireless power transfer (WPT) systems are good candidates to replace conventional wired power transfer methods in the future, because of their convenience and safety [1–3]. WPT systems have already been commercialized and applied to mobile applications, and an international standard has been established [4–6]. Research is also being actively conducted on how to apply a wireless charging system to electric vehicles (EVs), which is the current automobile trend [2,3,7]. The WPT system is not limited to simply transferring power, and a variety of methods to help automation of vehicles, which is another electric vehicle trend, are being studied [7,8]. In addition, many studies are being conducted to apply WPT systems to personal consumer applications such as drones [9] and to industrial automated guided vehicles (AGVs) [10].

In the WPT system, a transmitting (Tx) side and a receiving (Rx) side are electrically insulated, and power is transferred wirelessly through a magnetic field. To transfer power wirelessly, an electric current with a frequency of several tens of kHz to several MHz is used to form a strong magnetic field, and as a result there is high concern about magnetic field leakage [11]. Nearby humans can be exposed to the electromagnetic field (EMF) leaked from the WPT system, and various studies are being conducted to see how EMF affects the human body and how it can be reduced [12,13]. In addition, if there is an electronic device near the WPT system, the WPT system may cause electromagnetic interference

(EMI) problems in the device. Not only the fundamental of the operating frequency of the system, but also the odd or even harmonic components of the frequency, can cause EMI problems [14]. Various studies have also been conducted to solve the EMI problem caused by such a WPT system [11,15,16].

Systems that perform wireless charging after stopping, such as drones, AGVs, and EVs, have a high potential for misalignment between the Tx coil and the Rx coil. There are two types of misalignment. One is a lateral misalignment in which the Tx coil and the Rx coil are mismatched left and right [17], and the other type is a vertical misalignment in which the air gap between the Tx and Rx coils is different than the designed value. Various studies have been conducted on these two types of WPT coil misalignments. In addition, problems that appear when the coils are over-coupled, where they become closer than the designed value of the coils, have also been studied [14,18–20].

When over-coupling between coils occurs, the zero-phase angle (ZPA) of the equivalent input impedance of the WPT system is split into three points [18–20]. This is also called the frequency splitting phenomenon. When the ZPA is split into three points, it becomes very difficult to select an operating frequency for zero voltage switching (ZVS) for stable operation of the inverter [21]. In addition, when the ZPA is split into three points, the minimum value of the input impedance is split from one point into two points, and it is possible for the frequency of maximum power transfer (MPT) to also split into two points [20]. However, even if the frequency of MPT and ZPA are split, the maximum power transfer efficiency (PTE) has at the resonant frequency of the Rx side [20]. Since the frequency of the MPT and the frequency of the maximum PTE are different, it becomes very difficult to select a resonant frequency. One study proposed to automatically change the operating frequency of the inverter to the MPT frequency [22].

However, previous research studies on over-coupled WPT systems have two limitations. First, there is no study on the correlation between EMI and the over-coupling of WPT coils, which is known to be a major disadvantage of the WPT system, as described above. It can be inferred from the previously reported results that the input impedance changes according to the coupling between WPT coils. It can therefore be predicted that when the coupling changes, the magnitude of the current of the harmonic component also changes. However, none of the previous studies have linked the over-coupled WPT system and the EMI problem.

Another limitation of the previous studies is that there has been no study to closely adjust the frequency of the MPT and the frequency of the maximum PTE. The most significant problem with the frequency split phenomena is that the frequency of the MPT and the frequency of the maximum PTE are different. All of the studies up to this point have been limited to analyzing this phenomenon, but a study to adjust the above two frequencies is absolutely necessary.

This paper analyzes, first, how the over-coupled WPT system affects the harmonic currents. Next, the study examined how these harmonic currents change according to the coupling between the WPT coils, and finally, how the WPT system EMI problem changes depending on the coupling between the coils. In addition, factors affecting the design of additional series inductors to mitigate the various problems of an over-coupled WPT system were investigated. Various problems related to the over-coupled WPT system (the EMI issues, the difference between the MPT and PTE frequencies) were alleviated by applying the series inductor proposed in this paper. It was validated through simulations and experiments.

This paper is arranged as follows. In Section 2, after a brief review of the over-coupled WPT system, the correlation between EMI and the over-coupled WPT system is analyzed. In Section 3, considerations about designing series inductors are mentioned, and how they affect the over-coupled system is analyzed. In Section 4, the effects of the analyzed design considerations are demonstrated through simulation and experiments. After discussing the some contents of this paper in Section 5, and finally in Section 6, conclusions are presented.

2. Analysis of an Over-Coupled WPT System

There have been various basic studies of over-coupled WPT systems [14,18–20]. In this paper, we first analyze an over-coupled WPT system based on the previous research. In addition, the relationships between the slope of the input impedance and over-coupling, which have not been covered in previous studies, are analyzed. All of the analyses of the WPT systems in this paper were conducted assuming that a series–series (SS) compensation topology was used.

In a WPT system, a phenomenon in which the ZPA is split into three points instead of a single point due to the increase in the coupling coefficient (k) of the coils above a certain level is called the ZPA bifurcation. In this paper, a WPT system in which this phenomenon occurs is referred to as an over-coupled WPT system.

2.1. Criterion of an Over-Coupled WPT System

Before analyzing the over-coupled WPT system, it is necessary to look at the coupling coefficient at which over-coupling occurs. For this, the input impedance of the SS topology shown in Figure 1 is analyzed. In Figure 1, 'V_{in}' is the phasor form of AC input voltage, and 'C_{Tx}', 'L_{Tx}', 'R_{Tx}', 'C_{Rx}', 'L_{Rx}', and 'R_{Rx}' are the compensation capacitors, the inductance of the coils, and the resistance of Tx and Rx coils, respectively. In addition, 'k' represents the coupling coefficient between the Tx and the Rx coils as shown in Equation (1).

$$k = \frac{M}{\sqrt{L_{Tx} * L_{Rx}}} \tag{1}$$

'R_L' represents equivalent load. In most cases, the load resistance is much larger than that of the Rx coil, so the Rx coil should be included in the load resistance $(R_{Rx} + R_L \simeq R_L)$.
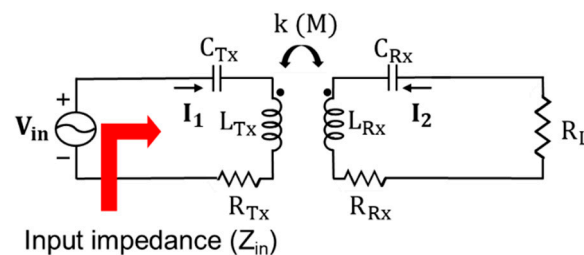

Figure 1. The equivalent circuit of a WPT system with an SS topology.

Based on this assumption, the input impedance of the WPT system with the SS topology viewed from the power source is as shown in Equation (2) under the conditions of Equations (3) and (4).

$$Z_{in} = R_{in} + jX_{in} = R_{Tx} + jX_{Tx} + \frac{\omega^2 M^2}{R_L + R_{Rx} + jX_{Rx}} \tag{2}$$

$$X_{Tx} = \omega L_{Tx} - \frac{1}{\omega C_{Tx}} \tag{3}$$

$$X_{Rx} = \omega L_{Rx} - \frac{1}{\omega C_{Rx}} \tag{4}$$

As described above, since the criterion for determining an over-coupled WPT system is established by the ZPA of the input impedance, the point where the phase of the input impedance becomes zero is calculated. The ZPA can be obtained as follows:

$$\angle Z_{in}(\omega) = \arctan\left(\frac{X_{in}}{R_{in}}\right) = 0 \tag{5}$$

The solution in Equation (5) is the same as in Equations (6) and (7) under the condition of Equation (8) if the values of electrical constants on Tx and Rx sides are identical [20]. In the process of calculating the frequency with the reactance component of Equation (2) as zero, Equation (6) is the solution to make all reactance on the Tx and Rx sides 0, so it is not related to the resistance values of the coils. However, the solutions in Equation (7) depend on the resistance of coils, load resistance, and coupling coefficient of the coil. In Equation (8), Q_2 is a quality factor on the Rx side. In the case of a WPT system with an SS topology, ZPA generally has three points. Figure 2 shows a conceptual graph where the ZPA is split into three points (ω_1, ω_2, ω_3) according to the coupling coefficient.

$$\omega_1 = \frac{1}{\sqrt{L_{Tx}C_{Tx}}} = \frac{1}{\sqrt{L_{Rx}C_{Rx}}} \tag{6}$$

$$\omega_2, \ \omega_3 = \omega_1 \sqrt{\frac{1 - 2Q_2^2 \pm \sqrt{1 - 4Q_2^2 + 4k^2Q_2^4}}{2\left(k^2 - 1\right)Q_2^2}}, \ (\omega_3 > \omega_2) \tag{7}$$

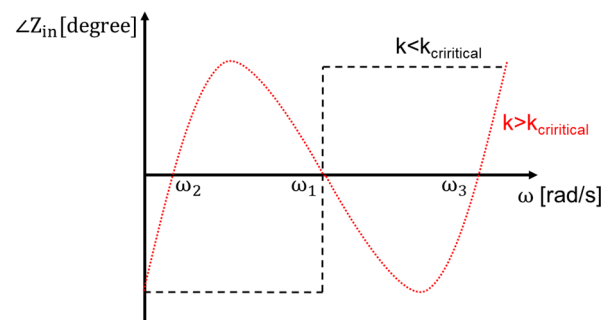$$Q_2 = \frac{1}{R_L}\sqrt{\frac{L_{Rx}}{C_{Rx}}} \tag{8}$$

Figure 2. Schematic diagram of the phase of the input impedance according to the coupling coefficient and frequency.

In order to mitigate the frequency split, the three frequencies of the ZPA must converge into one point. That one point should be the resonant frequency (ω_1) of the coil, which is the intentionally designed. First, among the ZPA's solutions, Equation (7) is converged to one point. This can be achieved as follows [20]:

$$1 - 4Q_2^2 + 4k^2Q_2^4 = 0 \tag{9}$$

$$k_{critical} = \frac{\sqrt{4Q_2^2 - 1}}{2Q_2^2} \tag{10}$$

The solution to Equation (9) is Equation (10) [20]. Equation (7) converged through Equation (9) is equivalent to the following [20]:

$$\omega_2 = \ \omega_3 = \omega_1 \sqrt{\frac{2Q_2^2 - 1}{2Q_2^2\left(1 - k^2\right)}} \tag{11}$$

In a typical WPT system, a high quality factor is selected to reduce loss, and the coupling coefficient between the Tx and Rx coils is usually less than 0.2 [23]. Therefore, the squared values of Q_2 and the coupling coefficient satisfy the conditions of Equations (12) and (13).

$$Q_2^2 \gg 1 \tag{12}$$

$$1 \gg k^2 \tag{13}$$

Therefore, in the case of a typical WPT system, the frequency of ZPA converges to one point as in Equation (14).

$$\omega_1 \simeq \omega_2 \simeq \omega_3, \tag{14}$$

The coupling coefficient with the condition of Equation (10) is called the critical coupling, and it is referred to as '$k_{critical}$' [20]. When the load resistance and the circuit constants including the coil are determined, $k_{critical}$ is determined. When the air gap between the coils becomes smaller and the coupling coefficient of the system increases more than $k_{critical}$, the ZPA is divided into three points and a frequency split phenomenon occurs.

2.2. Power Transfer Efficiency and Maximum Power Transfer of Over-Coupled WPT System

Over-coupled WPT systems differ from non-over-coupled systems in many ways. In this chapter, the power transfer efficiency (PTE) and maximum power transfer (MPT) of an over-coupled WPT system which have been previously analyzed are reviewed [19].

If the frequencies at which the reactance of the Tx and Rx sides become 0 are ω_{n1} and ω_{n2}, respectively, it can be expressed as Equations (15) and (16).

$$X_{Tx}|_{\omega=\omega_{n1}} = 0 \tag{15}$$

$$X_{Rx}|_{\omega=\omega_{n2}} = 0 \tag{16}$$

The PTE of the WPT system with an SS topology is as shown in Equation (17).

$$\eta = \frac{\omega^2 k^2 L_{Tx} L_{Rx} R_L}{R_{Tx}\left[(R_L + R_{Rx})^2 + X_{Rx}^2\right] + \omega^2 k^2 L_{Tx} L_{Rx} R_{Rx} + \omega^2 k^2 L_{Tx} L_{Rx} R_L} \simeq \frac{\omega^2 k^2 L_{Tx} L_{Rx} R_L}{R_{Tx}\left[(R_L + R_{Rx})^2 + X_{Rx}^2\right] + \omega^2 k^2 L_{Tx} L_{Rx} R_L} \tag{17}$$

As can be seen from Equation (17), the frequency of maximum PTE is the same as the Rx resonance frequency (ω_{n2}) at which X_{Rx} becomes zero. It can be concluded that the frequency of the maximum PTE is not affected by the coupling coefficient at all, as shown in Figure 3.
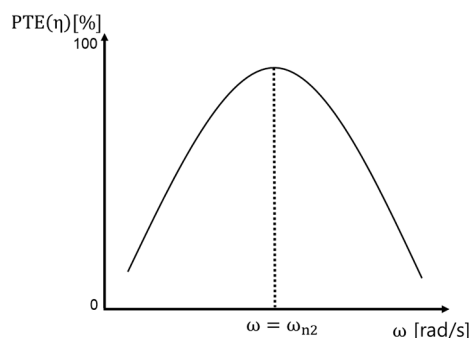
Figure 3. Schematic diagram of the power transfer efficiency of a WPT System.

Meanwhile, the MPT delivered to the load in the WPT system with an SS topology is as shown in Equation (18).

$$P_{out} = \frac{\omega^2 k^2 L_{Tx} L_{Rx} V_{in} R_L}{\left[R_{Tx}(R_{Rx} + R_L) - X_{Tx} X_{Rx} + \omega^2 k^2 L_{Tx} L_{Rx}\right]^2 + \left[R_{Tx} X_{Rx} + (R_{Rx} + R_L) X_{Tx}\right]^2} \tag{18}$$

Unlike the frequency of the maximum PTE, previous papers have reported that the frequency of the MPT is dependent on the coupling coefficient [19]. The frequency of MPT converges to the frequency of Equation (6) when the coupling coefficient is less than $k_{critical}$,

and diverges into the two frequencies of Equation (7) when it is greater than $k_{critical}$. This is shown in Figure 4.
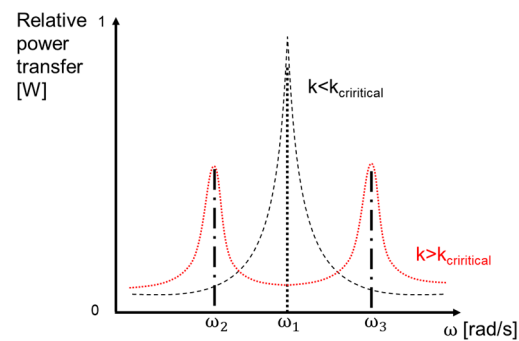

Figure 4. Schematic diagram of the transferred power to load according to the coupling coefficient and frequency.

As can be seen from the previous studies, the frequency of the maximum PTE in the over-coupled WPT system and the frequency of the MPT are different. In previous studies, in an over-coupled WPT system, the operating frequency was changed by tracking the frequency for MPT [22]. When the frequency splitting phenomenon occurs, the WPT system selects one of the split ZPAs as the operating frequency. In this paper, the higher frequency (ω_3) among the frequencies in Equation (7) was selected as the operating frequency. The reason can be seen in the phase graph in Figure 2. If the lower frequency is selected among the split frequencies (ω_2), the phase of the input impedance operates in the capacitive region ($\angle Z_{in} < 0°$) when the WPT coil is not over-coupled ($k < k_{critical}$). For the ZVS operation of the inverter [21], the phase of the input impedance must always operate in the inductive region ($\angle Z_{in} > 0°$), so a higher frequency ω_3 is used.

In other words, in an over-coupled WPT system, it is not possible to transfer power wirelessly with the highest efficiency at the frequency of MPT. In this paper, series inductors were applied to the WPT system to mitigate the difference between the two frequencies. Considerations involved in determining the additional series inductance value were also analyzed. Details on this will be analyzed in Section 3.

2.3. Analysis of Relation between the Over-Coupled WPT System and EMI

In this section, how the over-coupled WPT system affects EMI is analyzed. To analyze the EMI of the WPT coils, an analysis of the magnetic field of the circular coil must be conducted. The calculation of the magnetic field of the circular coil is shown in [24]. The calculation results are specified in Appendix A. As can be seen from Equations (A1)–(A3), when all geometric parameters are determined, the magnetic field caused by the circular coil depends on the magnitude of the current. The current in the coil is not only a component of the fundamental frequency of the WPT system, but also harmonic components (especially odd harmonics). Therefore, in order to mitigate the EMI of the WPT system, the current of the harmonic component must be reduced.

The current of a typical WPT coil varies according to the magnitude of the impedance, as shown in Equation (19).

$$|\mathbf{I_{coil}}(\omega)| = \left| \frac{\mathbf{V_{in}}(\omega)}{Z(\omega)} \right| \tag{19}$$

If the magnitude of the impedance in harmonics increases, the current will decrease, and the EMI issue will be improved. Therefore, it can be inferred that if the magnitude of the input impedance of Equation (2) in the harmonic of the WPT system is increased, the harmonic magnetic field will be reduced and the EMI issues of the WPT system will be improved.

The magnitude of the input impedance in Equation (2) is the same as that in Equation (20).

$$|Z_{in}| = \sqrt{R_{in}^2 + X_{in}^2} \tag{20}$$

However, at a frequency sufficiently higher than the resonant frequency ($\omega \gg \omega_1$), the relationship in Equation (21) is established. The magnitude of the input impedance considering the circuit constants of the Tx and Rx sides, respectively, is shown in Equation (22).

$$X_{in} \gg R_{in} \tag{21}$$

$$|Z_{in}| \simeq X_{in} = \frac{X_{Tx}\left(R_L^2 + X_{Rx}^2\right) - \omega^2 k^2 L_{Tx} L_{Rx} X_{Rx}}{R_L^2 + X_{Rx}^2} \tag{22}$$

Therefore, the slope of the input impedance according to operating frequency is equal to Equation (23).

$$\text{Slope of } |Z_{in}| \simeq \frac{\Delta X_{in}}{\Delta \omega} \tag{23}$$

Since the operating frequency of the WPT system is usually several tens of kHz to several MHz, when calculating the slope of the input impedance, the value can be approximated by using the coefficient of the highest order term in Equation (23). Considering Equations (21) and (22), approximating through the sixth order term, which is the highest frequency order in Equation (23), the slope of the magnitude of the input impedance with respect to frequency is equal to Equation (24).

$$\text{Slope of } |Z_{in}| \simeq \frac{\omega^6 \left(L_{Rx}^2 L_{Tx} - k^2 L_{Tx} L_{Rx}^2\right)}{\omega^6 L_{Rx}^2} \simeq L_{Tx}\left(1 - k^2\right) \tag{24}$$

That is, as the inductance of the coil of Tx increases and the coupling coefficient decreases, the magnitude of the slope increases. Figure 5 shows a schematic diagram of this result. Note that the condition in Equation (21) is meaningful only at a frequency that is sufficiently larger than the resonant frequency. Only then can Equation (23) be satisfied, and thus Equation (24) is satisfied only at a frequency greater than at least the third harmonic frequency of the fundamental frequency.
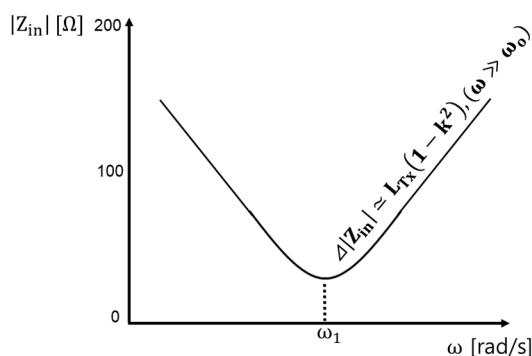

Figure 5. Schematic diagram of the input impedance according to the operating frequency.

Further analysis of Equation (24) shows that as the coupling coefficient increases, the slope of the input impedance with respect to the frequency decreases. If the two WPT systems have the same minimum impedance at the resonant frequency, the smaller the slope of the input impedance, the smaller the input impedance value at an arbitrary harmonic frequency. A conceptual graph explaining this in more detail is shown in Figure 6. Z_{in-1} and Z_{in-2} are the input impedances of the two systems, respectively, and k_1 and k_2 are the corresponding coupling coefficients. Since k_2 is greater than k_1 ($k_2 > k_1$), the slope of the magnitude of the input impedance of the k_2 system is smaller

than that of k_1 ($\Delta|Z_{in-1}| > \Delta|Z_{in-2}|$). Therefore, the input impedance of the system of k_2 at the frequency of the harmonic component is smaller than that of k_1 ($|Z_{in-1}| > |Z_{in-2}|$). In an over-coupled WPT system, since the coupling coefficient is higher than a certain level ($k_{critical}$), the coupling coefficient is relatively high, and the input impedance has a relatively low value at the frequency of the harmonic components.
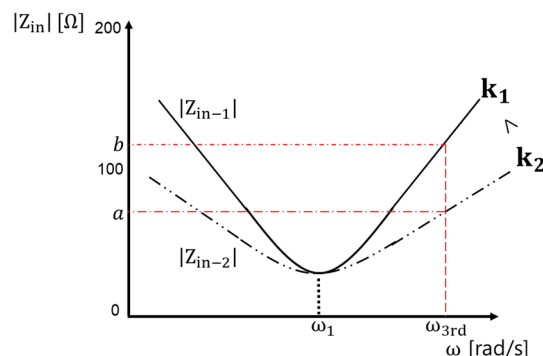

Figure 6. Conceptual graph of the input impedance of two systems depending on the value of coupling coefficients.

According to Equation (19), the magnitude of the low input impedance leads to a high harmonic current. Therefore, it is possible to deduce that when the coupling coefficient increases, the magnetic field in the harmonic component increases and an EMI problem occurs. In other words, the EMI problem worsens in an over-coupled WPT system with a relatively high coupling coefficient.

3. Factors to Consider When Designing a WPT System with Additional Series Inductors

In this paper, series inductors were connected to the Tx and Rx sides to improve the various issues of the over-coupled WPT system described in Section 2. The equivalent circuit of a WPT system with series inductors is shown in Figure 7. In Figure 7, L_{add-tx} and L_{add-rx} represent the inductance values series on the Tx side and Rx side, respectively, and R_{add-tx} and R_{add-rx} represent the resistance values of each of the series inductors. Other circuit constants are the same as in Figure 1. In fact, it is very common to add a series inductor as a filter to improve the EMI of electronic products [25]. In addition, there is a previous study which confirmed a reduction in EMI using series inductors in a WPT system [26]. However, the previous study was limited in two points. First of all, they did not analyze the factors used to determine the inductance value of the series inductors. In addition, it did not address how to improve performance by applying it to over-coupled WPT systems.
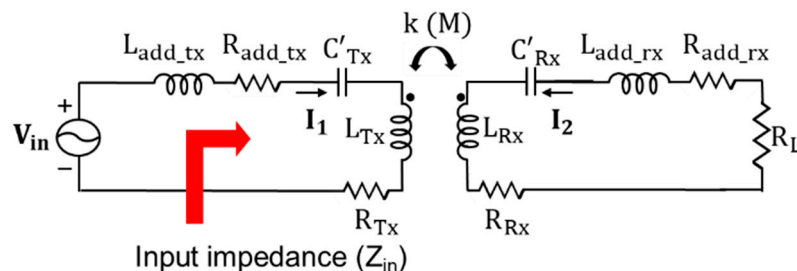

Figure 7. A WPT system with series inductors on the Tx and Rx sides.

This paper analyzes the effect of applying series inductors to an over-coupled WPT system. In the over-coupled WPT system with the additional series inductors, the frequency of the maximum PTE and the frequency of the MPT become close, enabling high power

transfer efficiency and high power transfer at the same time. In addition, when the series inductors were applied to an over-coupled WPT, the input impedance of the WPT system at the frequency of the harmonic component increased, and the EMI problem resulting from the magnetic field caused by the harmonic frequency was alleviated.

3.1. Resonant Frequency and Circuit Constant of WPT System with Series Inductors

The WPT system assumed in this paper is also applicable to applications which have a high potential of changing air gap, such as AGVs. Usually, the WPT system applied to AGV is designed to avoid the frequency split region. Therefore, as described in Section 2.2, the design is based on the condition that the operating frequency and the resonant frequencies of Tx and Rx are all the same ($\omega_1 = \omega_{n1} = \omega_{n2}$).

In a general WPT system that is not over-coupled, the resonances of the Tx and Rx sides are selected as shown in Equations (25) and (26). Equations (6), (25) and (26) are values that make the reactance components of Tx and Rx sides to zero, and are not related to the resistance component.

$$\omega_1 = \omega_{n1} = \frac{1}{\sqrt{(L_{add-tx} + L_{Tx})C'_{Tx}}} \tag{25}$$

$$\omega_1 = \omega_{n2} = \frac{1}{\sqrt{(L_{add-rx} + L_{Rx})C'_{Rx}}} \tag{26}$$

As shown in Equations (25) and (26), in a WPT system with series inductors, the compensation capacitances of Tx and Rx are selected considering these inductors. The transferred power and PTE graphs show the characteristics of Figures 3 and 4 because the compensation circuit is selected by considering the inductance values series to each side of Tx and Rx (L_{add-tx}, L_{add-rx}) and the inductance values of the coils (L_{Tx}, L_{Rx}). As shown in Figure 3, PTE has a maximum value only when the operating frequency is the same as the Rx side resonance frequency Equation (26), apart from over-coupling between coils. On the other hand, as shown in Figure 4, in the case of an over-coupled WPT system, the frequency of MPT is split into two points.

Before conducting the analysis of the WPT system with the series inductors, the circuit constant that changes after the inductor series is applied is newly defined, as shown in Table 1. The inductances on each side (L'_{Tx}, L'_{Rx}) and the equivalent resistances of the coils on each side (R'_{Tx}, R'_{Rx}) are defined by taking the values of the series inductors into account, and each reactance value (X'_{Tx}, X'_{Rx}) is also calculated by considering the series inductance value. Please note that the capacitance of the compensation circuit is calculated using Equations (25) and (26). Meanwhile, the newly defined coupling coefficient considering the added series inductors is defined as follows:

$$k' = M / \sqrt{L'_{Tx}L'_{Rx}} \tag{27}$$

Table 1. Defined circuit constants taking into account the series inductors.

Parameters	Defined		
L'_{Tx}	$L_{Tx} + L_{add-tx}$		
L'_{Rx}	$L_{Rx} + L_{add-rx}$	data	
R'_{Tx}	$R_{Tx} + R_{add-tx}$	data	
R'_{Rx}	$R_{Rx} + R_{add-rx}$		
X'_{Tx}	$\omega L'_{Tx} - \frac{1}{\omega C'_{Tx}}$		
X'_{Rx}	$\omega L'_{Rx} - \frac{1}{\omega C'_{Rx}}$		

In Equation (27), the mutual inductance is not related to the series inductors because it depends only on the coupling between the coils. In other words, the mutual inductance is not related to the series inductors.

3.2. Analysis of the MPT and PTE of the WPT System with Series Inductors

The PTE according to frequency change was analyzed when series inductors were applied to the Tx and Rx sides. It should be noted that in Equation (17), not only the resistance of the coil but also the resistance of the series inductance must be included. If this is expressed again in the equation, it is equal to Equation (28).

$$\eta = \frac{\omega^2 k' L'_{Tx} L'_{Rx} R_L}{R'_{Tx}\left[\left(R_L + R'_{Rx}\right)^2 + X'^2_{Rx}\right] + \omega^2 k' L'_{Tx} L'_{Rx} R'_{Rx} + \omega^2 k' L'_{Tx} L'_{Rx} R_L} \tag{28}$$

Therefore, when designing a WPT system with series inductors, modeling of the series inductors is very important. Inductance and resistance calculations through modeling of toroidal inductors have been performed in various previous studies [27–29]. One is a method using mathematical calculation [27,28], and the other is a calculation method using a magnetic field EM simulator [29]. In either case, when calculating the PTE in a WPT system including series inductors, not only the inductance of the series inductor, but also the resistance must be reflected in the calculation of Equation (28).

Second, the change in MPT according to the frequency of the WPT system, including the series inductors, was analyzed. As can be seen from Equation (11), when the equivalent inductance of R_x $(L'_{Rx} = L_{Rx} + L_{add-rx})$ increases, the two divided frequencies ω_2 and ω_3 become closer to one point of ω_1. That is, the frequencies (ω_2, ω_3) with the MPT approach the frequency with the maximum efficiency (ω_1) as shown in Figure 8. It can be concluded that the series inductors improve the difference between the frequency of the MPT and the frequency of maximum PTE as the coupling coefficient increases, which is one of the biggest drawbacks of the over-coupled WPT system.
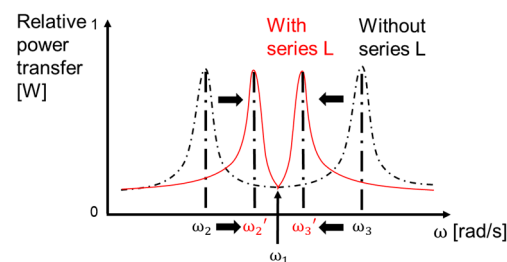

Figure 8. A conceptual graph showing the change in the MPT frequency according to the presence or absence of inductors.

3.3. EMI in the WPT System with Series Inductors

As mentioned in Section 2.3, the electromagnetic field of the WPT system is proportional to the current in the Tx and Rx coils, and the method to reduce the harmonic components current is key to improving the EMI problem of a WPT system. In order to reduce the harmonic component current, the magnitude of the impedance at the harmonic frequency must be increased.

The current of the Tx coil is determined by the magnitude of the input impedance. This can be expressed as follows:

$$|\mathbf{I}_1(\omega)| = \left|\frac{\mathbf{V_{in}}(\omega)}{Z_{in}(\omega)}\right| \tag{29}$$

Note that the condition in Equation (29) is that the input voltage is constant. As the inductance of the Tx side increases, the slope of the inductance magnitude increases.

Therefore, when a series inductor (L_{add-tx}) is applied to the Tx side, the impedance of the harmonic component, which is sufficiently higher than the natural resonance frequency ($\omega \gg \omega_1$), increases, as shown in Figure 9. Therefore, the current of the harmonic component decreases. The series inductors on the Tx side reduce the current in the Tx coil, and it can be inferred that the EMI issues will also be mitigated, as shown in Appendix A.
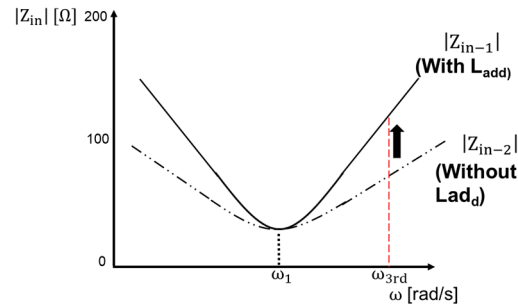

Figure 9. Equivalent input impedance of Rx side viewed from Rx equivalent source.

Similarly, the current in the Rx side coil is equal to Equation (30).

$$|\mathbf{I}_2(\omega)| = \left| \frac{\mathbf{V}_2(\omega)}{Z_{in-rx}(\omega)} \right| \tag{30}$$

The difference between the current on the Rx side and the current on the Tx side is that $\mathbf{V}_2$ is the voltage induced by the Tx side current ($\mathbf{I}_1$). This can be seen in Figure 10, and the equivalent impedance viewed from the equivalent power source ($\mathbf{V}_2$) of Rx is as follows:

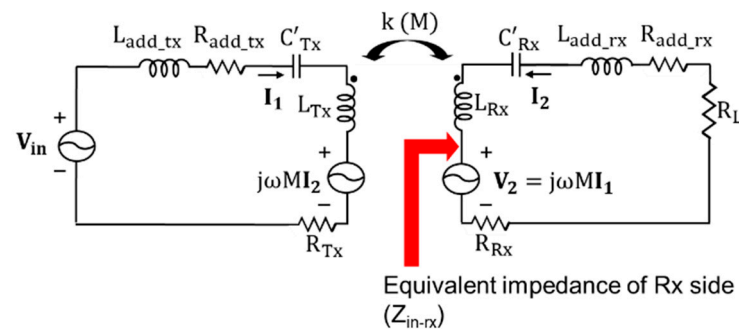$$Z_{in-rx}(\omega) = R_L + R'_{Rx} + jX'_{Rx}. \tag{31}$$

Figure 10. Equivalent input impedance on the Rx side, viewed from an Rx equivalent source.

At a frequency sufficiently greater than the natural resonance frequency ($\omega \gg \omega_1$), the magnitude of input impedance is as follows:

$$|Z_{in-rx}(\omega)| \simeq X'_{Rx}. \tag{32}$$

At a frequency sufficiently greater than the natural resonance frequency ($\omega \gg \omega_1$), Equation (32) increases as L'_{Rx} increases, so when L_{add-rx} is a series, the magnitude of equivalent impedance on the Rx side ($|Z_{in-rx}(\omega)|$) in harmonic component also increases, as shown in Figure 9. Likewise, since the current in the harmonic component causing the EMI issue decreases as the impedance increases, it can be inferred that L_{add-rx} also alleviates the EMI issue.

3.4. Considerations on Desgining a WPT System with Additional Series Inductors

Based on the analyses, as the additional series inductance increases, the effect on the MPT, the magnitude of the impedance, and the PTE are as summarized in Table 2. When the series inductance increases, the frequency of the MPT approaches the resonant frequency of the maximum PTE, and the magnitude of the input impedance increases, thereby reducing the harmonic component current, improving the EMI issue. However, as the series inductance increases, the resistance of the series inductance also tends to increase, resulting in a lower PTE.

Table 2. Advantage and disadvantage of applying additional series inductors.

Components	Change as Added Inductance Increases	
Frequency of MPT	Approaching to ω_o (Advantage)	data
Magnitude of impedance	Higher magnitude of Z_{in} in harmonics (Advantage)	data
PTE at natural resonance frequency	Lower power transfer efficiency (Disadvantage)	

Figure 11 shows the considerations when designing a WPT system with series inductors. First, when designing a WPT system with the possibility of a changing air gap, check the coupling coefficient that can be maximized (k_{max}). If the maximum coupling coefficient (k_{max}) is less than the critical coupling coefficient ($k_{critical}$), the series inductors can be designed only to improve EMI. On the other hand, if the maximum coupling coefficient (k_{max}) is greater than the critical coupling coefficient ($k_{critical}$), series inductors should be designed both to bring the frequency of the MPT close to the frequency of the maximum PTE and to improve the EMI issue. Finally, efficiency must be considered in all cases. The series inductors in the WPT system must be properly selected based on the importance of efficiency and EMI issues, MPT frequency and maximum PTE frequency.
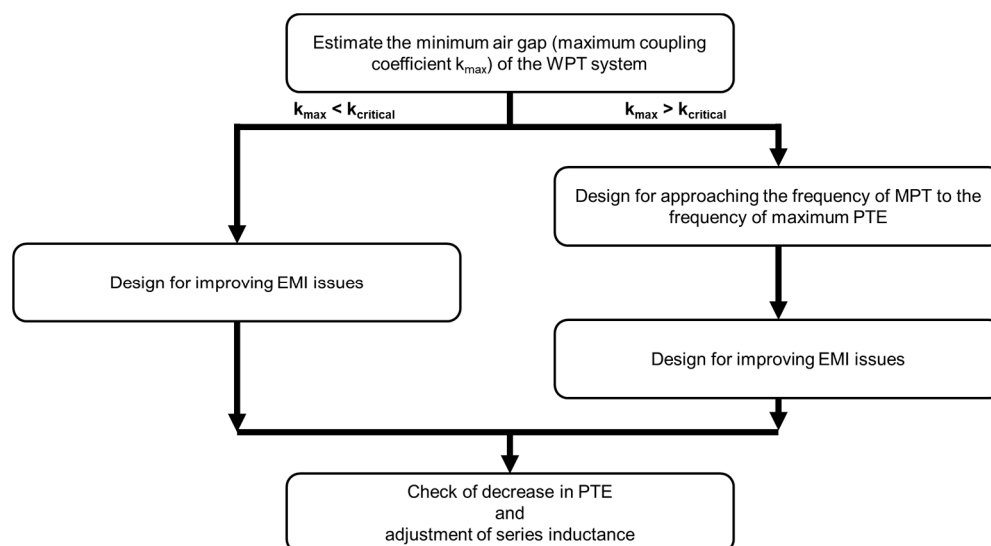

Figure 11. Design considerations of series inductors according to the maximum coupling coefficient of the WPT system.

4. Verification through Simulations and Experiments

4.1. Simulation Results

Figure 12 shows the structure of the WPT coils designed using an electromagnetic (EM) field simulator. The contents proposed in this paper were verified using the coil in Figure 12. The design specifications of the coils on the Tx and Rx sides are the same. The structural information of the coil and the wire is specified in Table 3. In addition, the simulation results are shown in Table 4. The resonance frequency was selected to be

60 kHz, and the mutual inductance values and coupling coefficient according to the air gap are listed in Table A2 in Appendix B.
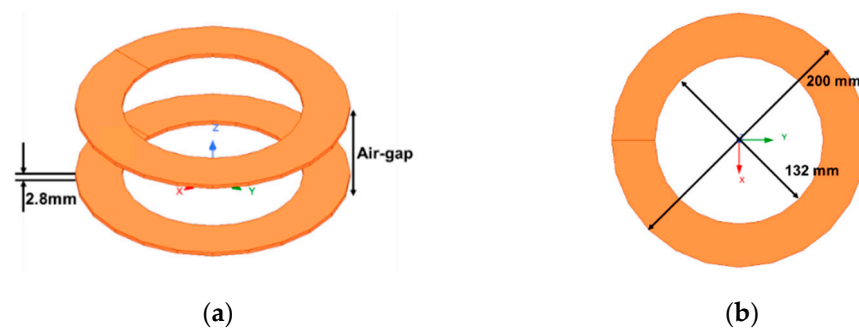

Figure 12. WPT coils designed by an electromagnetic field simulator: (**a**) bird's eye view; (**b**) top view.

Table 3. Structural and material specifications of WPT coils.

Parameters	Value	
Wire of coil	0.05 mm/1300 strands Litz wire	data
Diameter of the wire	2.8 mm	data
Layer of coil	1 layer	
Number of turns	12 turns	

Table 4. EM simulation results of coils.

Parameters	Value	
Frequency	60 kHz	
Inductance	35.6 μH	data
Resistance	43 mΩ	

First, the magnitude of the input impedance according to the coupling coefficient analysis was analyzed. The circuit simulation was conducted with the configuration shown in Figure 1, and the magnitude of the input impedance was analyzed as the coupling coefficient (k) changed. Information on the detailed setup of the circuit simulation is shown in Table 5.

Table 5. Setup of circuit simulations.

Parameters	Value	
Resonance frequency (ω_{n1}, ω_{n2})	60 kHz	
Tx and Rx coils inductance (L_{Tx}, L_{Rx})	35.6 μH	data
Resistance of coils (R_{Tx}, R_{Rx})	43 mΩ	
Compensation capacitor of Tx and Rx side (C_{Tx}, C_{Rx})	197.6 nF	
Coupling coefficient (k)	0.10~0.51 (5 steps) [1]	
Load resistance (R_L)	2.4 Ω	

[1] Corresponding coupling coefficient according to air gap change (5 steps from 20 mm to 100 mm in 20 mm steps) in Table A2.

Figure 13 shows the changes in the magnitude and phase of the input impedance, respectively. As expected in Section 2.3, as the coupling coefficient increases, the slope of the input impedance decreases. Since the slope of the input impedance decreases, the magnitude of the input impedance also decreases in the harmonic components. This is shown in Figure 13a. In addition, as expected in previous studies, as the coupling coefficient increases, the ZPA gradually moves away from the original resonance frequency of 60 kHz.

This is shown in Figure 13b. Note that the critical coupling coefficient ($k_{critical}$) obtained using Equation (10) is 0.176.
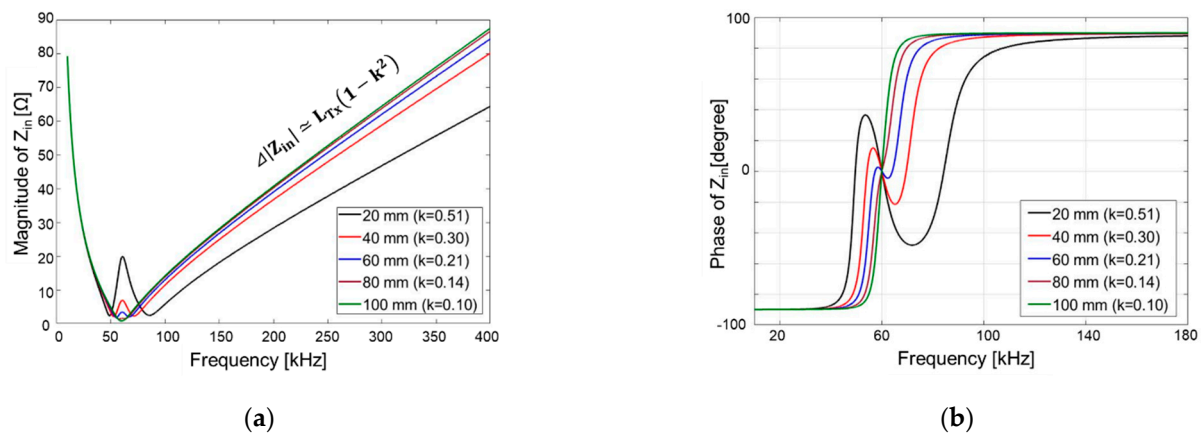

(**a**)

(**b**)

Figure 13. Change in input impedance according to air gap (coupling coefficient): (**a**) input impedance magnitude change according to frequency change; (**b**) input impedance phase change according to frequency change.

Next, the effect on the WPT system with series inductors was analyzed. As mentioned above, the calculation of the inductor is divided into a method using calculation [27,28] and an analysis method using an EM solver [29]. In this paper, the inductor was designed using a toroidal core, and the inductance and resistance values of the inductor were calculated using an EM solver. Detailed design information about the inductors is presented in Appendix C.

As described in Section 3, not only the inductance of the series inductor, but also the resistance of the series inductor is very important, and the calculation results are shown in Table A4. The circuit simulation was configured as shown in Figure 7 and the basic circuit simulation setup is shown in Tables 6 and 7. The coupling coefficient was selected to be 0.37 for a 30 mm air gap in Table A2. The capacitance of the compensation circuits (C'_{Tx}, C'_{Rx}) was calculated by considering the resonance frequency and the equivalent inductance of each Tx and Rx (L'_{Tx}, L'_{Rx}) and is calculated through Equations (25) and (26).

Table 6. Setup for circuit simulation of changing input impedance according to L_{add}.

Parameters	Value
Resonance frequency (ω_{n1}, ω_{n2})	60 kHz
Tx and Rx coils inductance (L_{Tx}, L_{Rx})	35.6 µH
Resistance of coils (R_{Tx}, R_{Rx})	43 mΩ
Coupling coefficient (k)	0.37
Load resistance	2.4 Ω

Figure 14 shows the change in the input impedance as the series inductance changes. Figure 14a shows the magnitude of the input impedance. As expected from Equation (24), as the inductance value of the series inductors increases, the input impedance at the frequency of the harmonic component increases. Since L_{add-tx}, L_{add-rx} are increased in units of 10 µH, the slope of the input impedance increased very regularly, as expected in Equation (24). In addition, as can be seen from Figure 14b, as the value of the series inductance increases, the ZPA frequencies (ω_1, ω_2, ω_3) converge to the original resonance frequency (ω_1) of the system. Particularly, as described in Section 3, when the WPT system is over-coupled and a frequency splitting phenomenon occurs, ω_3 is used as the operating frequency. It has been determined that ω_3 is the frequency of the MPT. On the other hand, as described in Section 3, the frequency of the maximum PTE is the original resonant frequency (ω_1) of the system. Therefore, ω_3 getting closer to ω_1 means that the frequency

of maximum PTE and the frequency of MPT are getting closer, which can improve the disadvantages of the conventional over-coupled WPT system. In an over-coupled WPT system, the difference between the frequency of maximum PTE ($\omega_1 = 2\pi f_1$) and the frequency of MPT ($\omega_3 = 2\pi f_3$) is defined as follows:

$$\Delta f = f_3 - f_1. \tag{33}$$

Table 7. Inductance of series inductors (L_{add}) and corresponding compensation capacitance values (C_{Tx}, C_{Rx}).

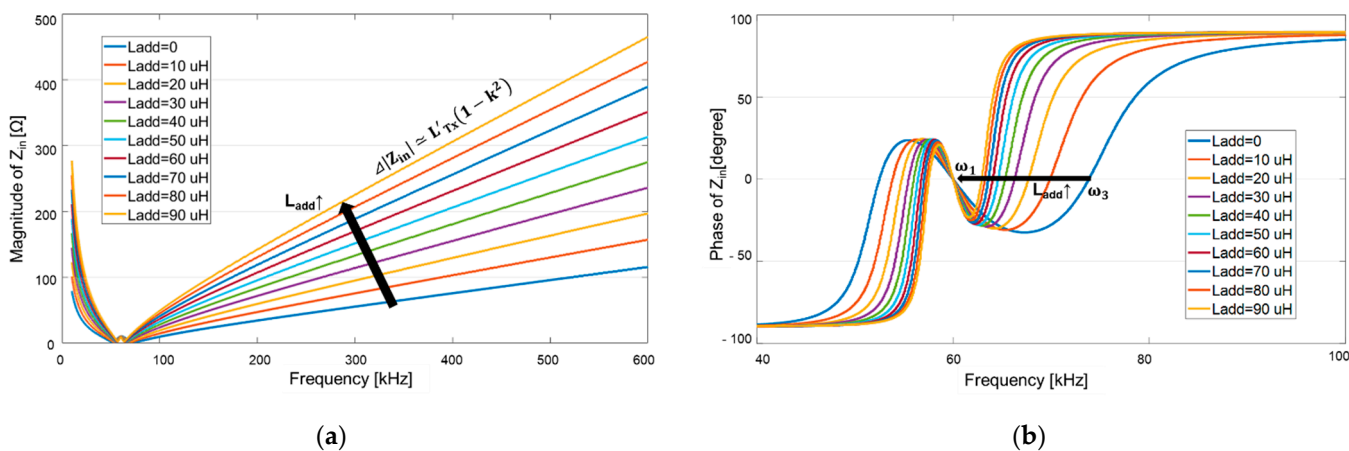| Inductance of Coils (L_{Tx}, L_{Rx}) [µH]	Series Inductance (L_{add-tx}, L_{add-rx}) [µH]	Compensation Capacitance (C'_{Tx}, C'_{Rx}) [nF]
	0	195.5
	10	152.9
	20	126.6
	30	107.2
35.6	40	93.1
	50	82.2
	60	73.6
	70	66.6
	80	60.9
	90	56.3

(a)

(b)

Figure 14. Input impedance change according to the series inductance value (L_{add-tx}, L_{add-rx}): (**a**) input impedance magnitude change according to frequency change; (**b**) input impedance phase change according to frequency change.

Figure 15 shows the PTE and the relative power transferred to the load as a function of the additional series inductance. Here, PTE is the ratio of the power delivered to the equivalent load (R_L) to the power supplied from the power source (V_{in}), and the power transfer capacity is the relative amount of power transferred to the equivalent load (R_L) in the setup in Figure 7. The relative amount of transferred power means the ratio when the maximum transferred power is set to unity. As shown in Figure 15a, it always has the maximum efficiency at the resonant frequency regardless of the inductance value of L_{add}. This is what was expected in Equation (17). As the value of L_{add} is increased, the overall efficiency decreases due to the parasitic resistance (R_{add-tx}, R_{add-rx}) of L_{add}. Figure 15b shows the relative power transfer capacity according to series inductance. As expected from the impedance phase in Figure 14b, the frequency (ω_2, ω_3) of MPT gradually approaches ω_1 as the series inductance increases. Note that the relative MPT gradually decreases as series inductance increases. This is a reasonable result considering that all parasitic resistance values are located in the denominator in Equation (18).
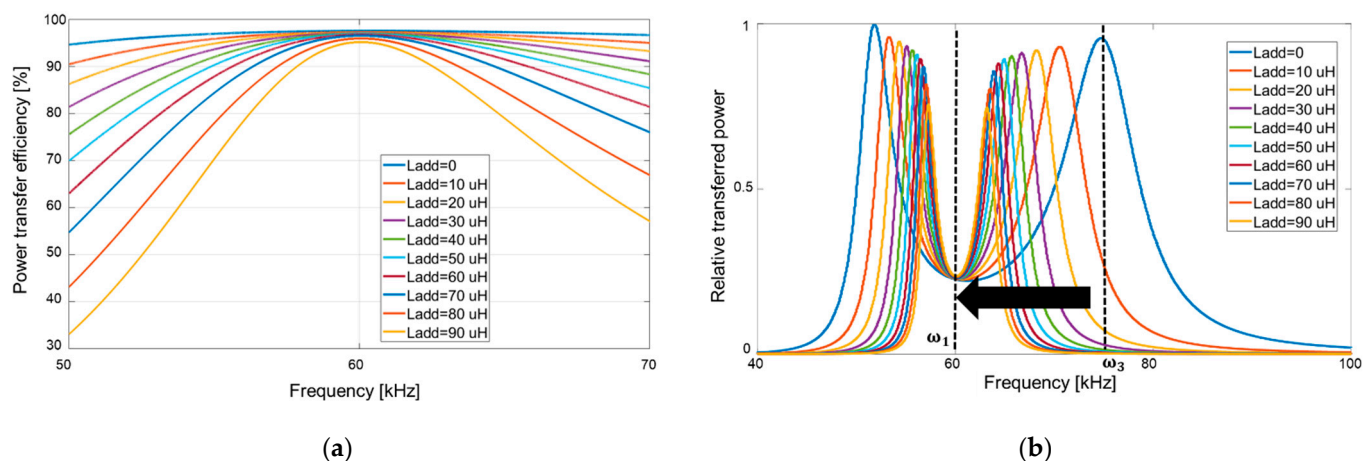
(**a**)

(**b**)

Figure 15. PTE and relative transferred power to load change according to the series inductance value (L_{add-tx}, L_{add-rx}): (**a**) change in PTE according to frequency change; (**b**) change in relative transferred power according to frequency change.

Figure 16a shows the difference between the maximum PTE frequency in Figure 15a and the MPT frequency in Figure 15b. As previously analyzed, the difference between the two frequencies decreases as the series inductance value increases. Meanwhile, Figure 16b shows that the power transfer efficiency decreases as the series inductor increases.
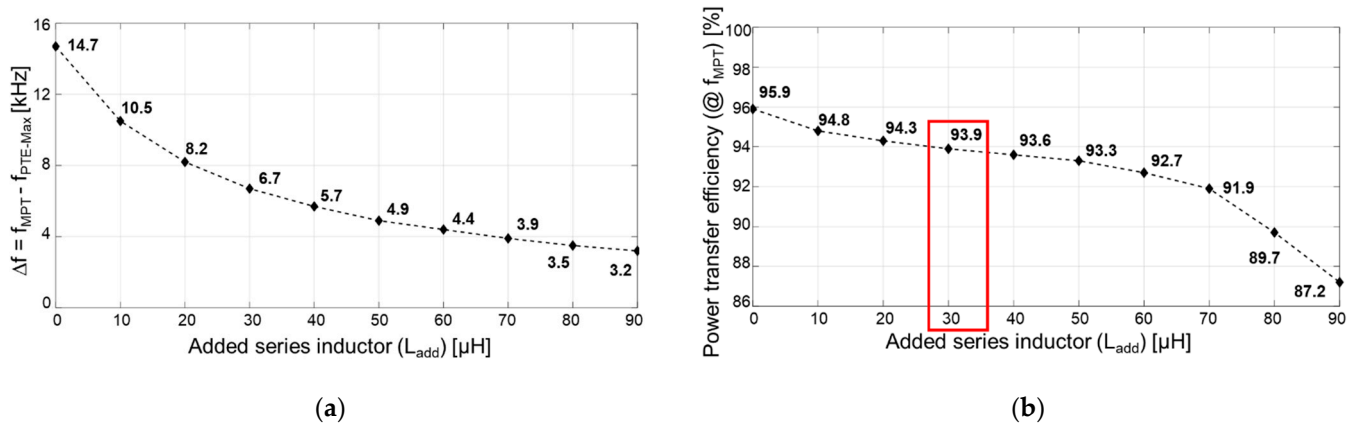

(**a**)

(**b**)

Figure 16. The difference between the MPT frequency and the maximum PTE frequency, and the power transfer efficiency change at the MPT frequency according to the change in the series inductor (L_{add-tx}, L_{add-rx}): (**a**) change in the difference between the MPT frequency and the maximum PTE frequency (Δf); (**b**) change in the power transfer efficiency change at the MPT frequency.

Additionally, Figure 17 shows the fast Fourier transform (FFT) results at the fundamental frequencies of the Tx current and Rx current and the third, fifth, and seventh harmonic frequencies when the circuit simulation of the 30 W class WPT system was conducted. As expected from Section 2, the input impedance increased as the inductance of the series inductor increased, so that the current in the harmonic frequency component decreased. As the series inductance increases, the magnitude of the current decreases at the frequencies of all harmonics except the fundamental component. Meanwhile, as the series inductance increases, the MPT decreases slightly, as shown in Figure 15b, so in order to transfer the same power (30 W), the fundamental component of the Tx current must increase slightly, which is shown in Figure 17a. Since the output power is all the same at 30 W, the fundamental of the Rx current is the same, which is also shown in Figure 17a.
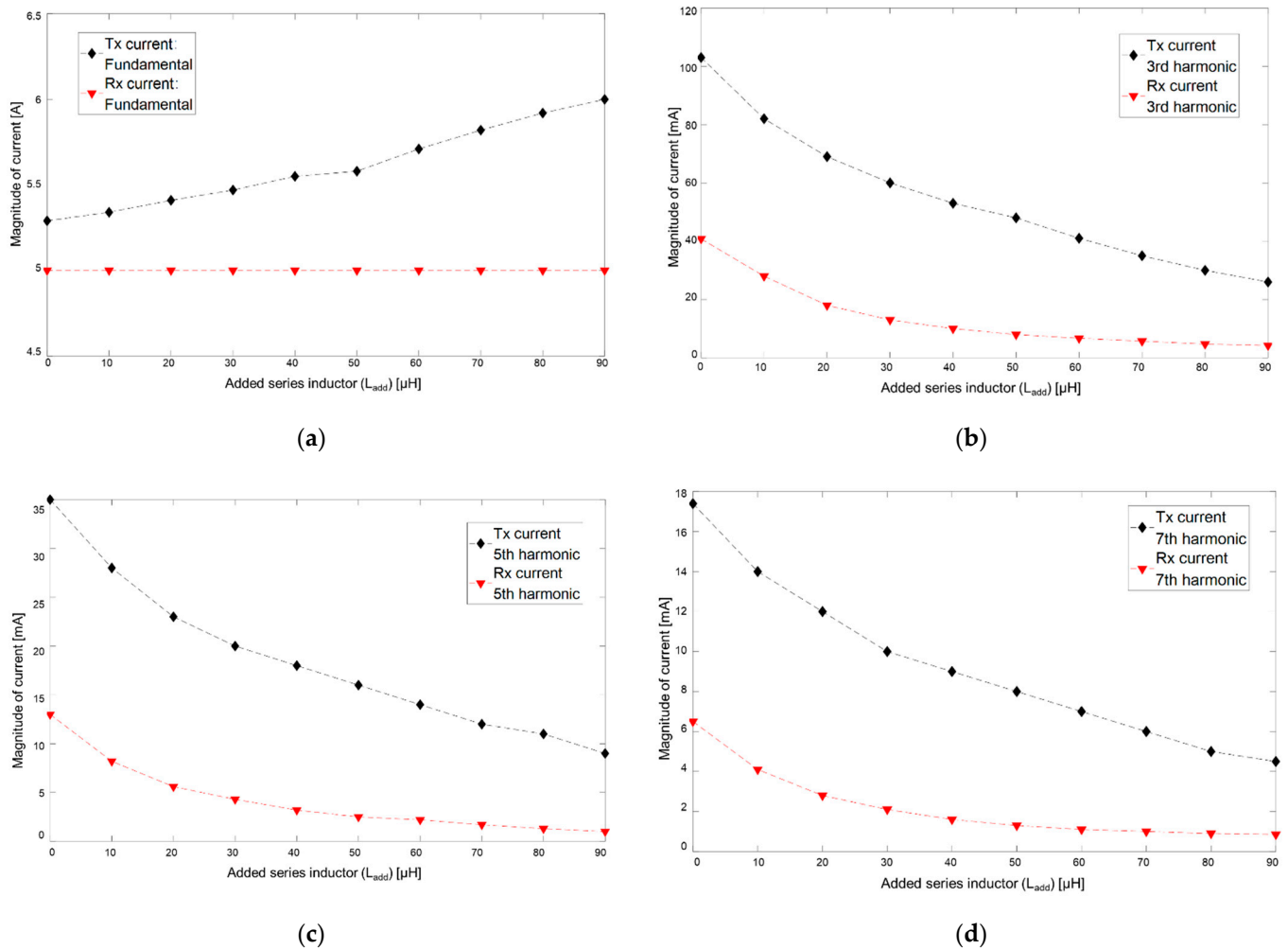
Figure 17. Changes in current harmonic components according to the value of the additional series inductors (L_{add-tx}, L_{add-rx}): (**a**) fundamental components of Tx and Rx currents; (**b**) 3rd harmonic components of Tx and Rx currents; (**c**) 5th harmonic components of Tx and Rx currents; (**d**) 7th harmonic components of Tx and Rx currents.

In this paper, the additional series inductor was selected to be 30 µH. The PTE of the WPT system decreases by 2% or less compared to when the series inductor is not added. It is up to the WPT system designer to choose whether to focus on efficiency or EMI in a WPT system.

In order to analyze the components of the current harmonics of the WPT system including the designed L_{add}, a power transfer circuit simulation setup was constructed, as shown in Figure 18. All circuit simulation parameters except the load resistance were configured as shown in Tables 4 and 5. The load resistance was set to 3 ohms so that the input resistance considering the rectifier was equivalent to 2.4 ohms, as shown in Figure 18 [21]. The input power P_{in} is the real power output from the inverter, and the output power P_{out} is the real power input to the rectifier, as also shown in Figure 18.
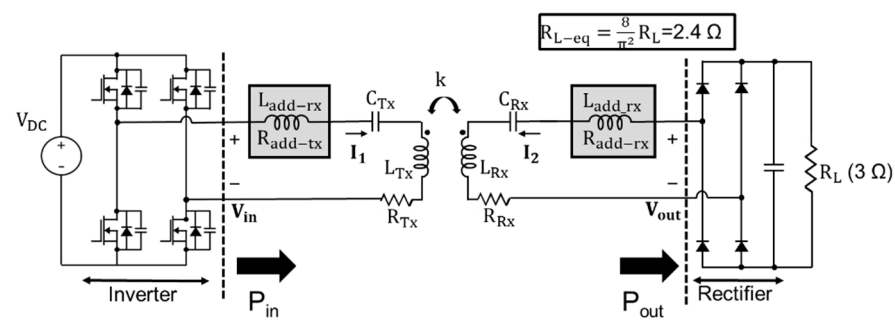
Figure 18. Circuit simulation setup for current harmonic component analysis according to L_{add}.

Table 8 shows the simulation results when operating a 30 W class WPT system. As previously targeted, it can be seen that the PTE of the WPT system with the series inductor added is 2% lower than that of the system without the series inductor added.

Table 8. Simulation results of a 30 W class WPT system according to the presence of L_{add} (30 μH).

Parameters	Without L_{add}	With L_{add} (30 μH)
Input voltage (V_{in})	9.8 V_{rms}	10.3 V_{rms}
Input current (I_1)	3.74 A_{rms}	3.87 A_{rms}
Input power (P_{in})	31.5 W	32.1 W
Output voltage (V_{out})	8.5 V_{rms}	8.5 V_{rms}
Output Current (I_2)	3.74 A_{rms}	3.54 A_{rms}
Output Power (P_{out})	30.2 W	30.15 W
Power transfer efficiency (P_{out}/P_{in})	95.87%	93.93%

4.2. Experiment Results

For the measurement, WPT coils to be used in the WPT system are fabricated. The manufactured coil has design specifications as shown in Figure 12 and Tables 3 and 4, and the actual shape is shown in Figure 19, and the measured electrical data are shown in Table 9.

Figure 19. Fabricated actual WPT coils.

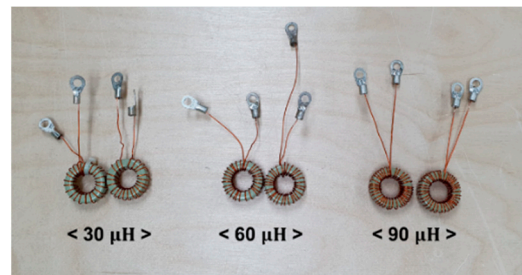**Table 9.** Measured inductance and resistance of the WPT coils.

Parameters	Inductance [μH]	Resistance [Ω]
Coil 1	35.4	0.059
Coil 2	35.5	0.054

In addition, Table 10 shows the mutual inductance and the coupling coefficient at each air gap of the coils of the WPT system.

Table 10. Measured inductance and resistance of WPT coils.

Air Gap between Tx and Rx Coils [mm]	Inductance [μH]	Coupling Coefficient
30	14.33	0.40
60	8.00	0.26
90	4.75	0.13

Next, toroidal inductors were fabricated for the series inductors. The toroidal cores had the design specifications shown in Table A3 in Appendix C. The shape of the actual fabricated core is shown in Figure 20, and the calculated resistance values and measured resistance values at each inductance are shown in Table 11. The toroidal inductances for the experiments were produced by selecting three representative values (30 μH, 60 μH, 90 μH) from the series inductance values (10 to 90 μH) used in the simulation in Table 7. Although there was a difference of up to 30% between the measured resistance value of the inductor and the resistance value calculated by the EM solver, it can be concluded that the calculation of the resistance value by the EM solver is reliable enough to design an actual WPT system.

Figure 20. Toroidal inductors manufactured for use as series inductors.

Table 11. Measured resistance and calculated resistance value of the manufactured inductor.

Inductance [μH]	Calculated Resistance [Ω]	Measured Resistance [Ω]
30	0.050	0.066
60	0.081	0.116
90	0.258	0.370

Meanwhile, Table 12 shows the value of the compensation capacitance selected using (25) and (26) according to the inductance value of the coil and the inductance value of the series inductors.

Table 12. Inductance of series inductors (L_{add}) and corresponding compensation capacitance values (C'_{Tx}, C'_{Rx}).

Inductance of Coils (L_{Tx}, L_{Rx}) [μH]	Series Inductance (L_{add-tx}, L_{add-rx}) [μH]	Compensation Capacitance (C'_{Tx}, C'_{Rx}) [nF]	Resonance Frequency [kHz]
	0	200	59.73
35.5	30	107	60.12
	60	74	59.87
	90	56	59.98

Using the fabricated and measured WPT coils, series inductors, and compensation capacitors, the setup was constructed as shown in Figure 7 and the input impedance was measured. The load resistance (R_L) was selected to be 2.4 ohms as in the simulation, and the inductance of the load resistor was less than 10 nH, so it had little effect on the resonance of

the WPT system. The input impedance was measured as shown in Figure 21; an impedance analyzer (Keysight E4990A) was used for the measurement.
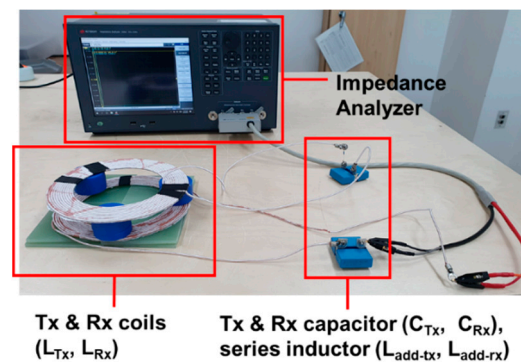

Figure 21. Input impedance measurement using an impedance analyzer.

First, the slope and phase of the input impedance change were measured according to the coupling coefficient. The input impedance was measured by changing the air gap between the WPT coils to 30, 60, and 90 mm, and the result is shown in Figure 22. As in the simulation conducted above, it can be seen from Figure 22a that the smaller the air gap between the coils (the larger the coupling coefficient of the coils), the smaller the slope of the input impedance and the smaller the magnitude of the input impedance in the harmonic components. In addition, it can be seen from Figure 22b that as the coupling coefficient increases, the ZPA frequencies (f_2, f_3) gradually become farther from the original resonant frequency ($f_1 = 60$ kHz).
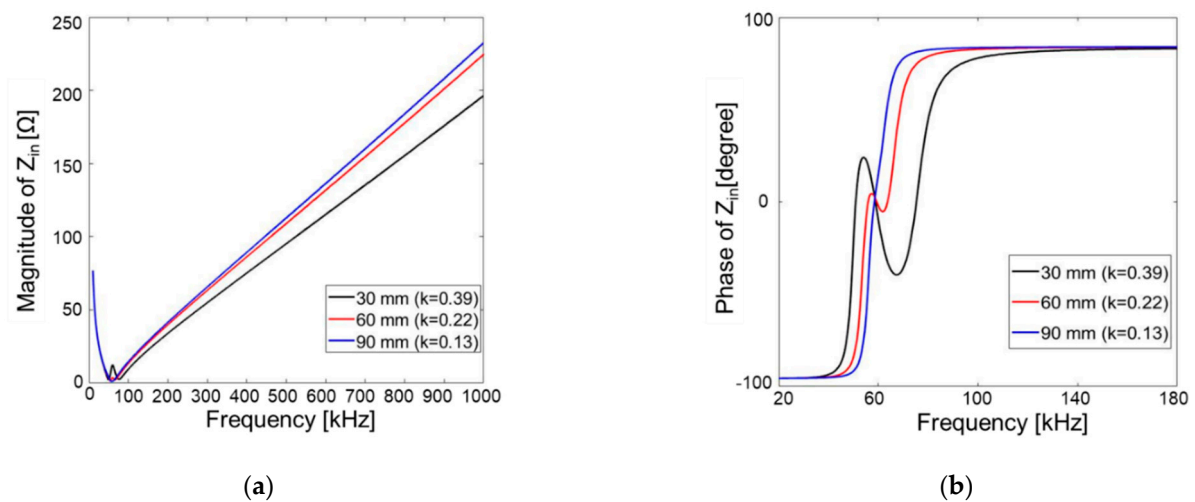

| (a) | (b) |

Figure 22. Measured input impedance according to air gap (coupling coefficient): (**a**) input impedance magnitude change according to frequency change; (**b**) input impedance phase change according to frequency change.

Figure 23 shows the change in the input impedance when the series inductors were added to the WPT system. As in the simulation, as the series inductance value increased, both the slope of the magnitude of input impedance and the magnitude of impedance at the harmonic component frequency increased, as shown in Figure 23a. Likewise, it can be seen from Figure 23b that as the series inductance increased, the frequencies of ZPA (f_2, f_3) rather than the resonant frequency gradually approach the original resonant frequency ($f_1 = 60$ kHz).
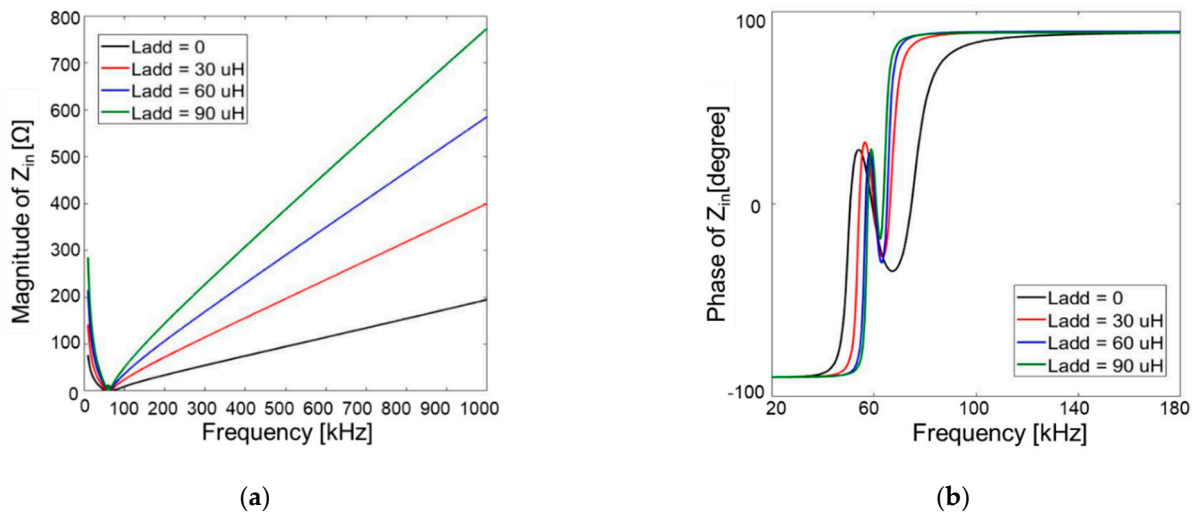
(**a**)

(**b**)

Figure 23. Measured input impedance change according to the series inductance value (L_{add-tx}, L_{add-rx}): (**a**) input impedance magnitude change according to frequency change; (**b**) input impedance phase change according to frequency change.

Figure 24 shows the experimental setup used for measuring the current harmonics and transferred power of a WPT system. Measurements were performed using an oscilloscope (Keysight MSO-X4154A) and a power analyzer (YOKOGAWA WT1802E). Input and output power were measured based on Figure 18, from the output of the inverter (P_{in}) to the input of the rectifier (P_{out}). Table 13 shows the voltage, current, and power of the input, output, respectively, with and without series inductance when performing a 30 W class WPT experiments. Compared to the WPT in the previous simulation, the PTE decreased by 4.5% both with and without the series inductance. For that reason, first, the resistance of the compensation capacitor was ignored in the simulation, but the parasitic resistance of the actual compensation capacitor was about 20 to 40 mΩ, which cannot be ignored, compared to the resistance of the WPT coils (about 50 mΩ). The second reason is that the resistance of the fabricated coil and the series inductor was measured to be slightly higher than that of the simulation. However, as in the simulation, the difference between the measured PTE with and without the series inductor was less than 2%, so it can be concluded that the design considerations of the WPT system with the series inductor analyzed in this paper are valid.
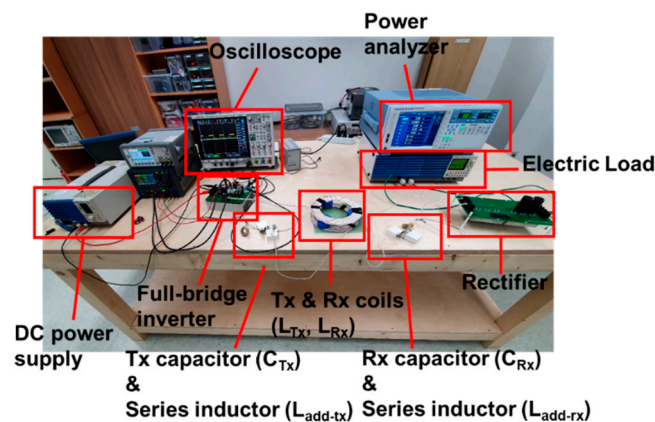

**Figure 24.** Experimental setup for measuring the transferred power and harmonics of current in a WPT system.

Table 13. Experimental results of a 30 W class WPT system according to the presence of L_{add} (30 μH).

Parameters	WO L_{add}	With L_{add} (30 μH)
Input voltage (V_{in})	14.2 V_{rms}	14.7 V_{rms}
Input current (I_1)	4.00 A_{rms}	4.15 A_{rms}
Input power (P_{in})	36.5 W	36.4 W
Output voltage (V_{out})	10.73 V_{rms}	10.4 V_{rms}
Output Current (I_2)	3.41 A_{rms}	3.44 A_{rms}
Output Power (P_{out})	33.3 W	32.5 W
Power transfer efficiency (P_{out}/P_{in})	91.23%	89.29%

Table 14 shows the peak values of the fundamental components among the current components of the Tx and Rx coils. As in the previous simulation, the fundamental component of the Tx coil current when the series inductance was applied is higher than when the series inductance was not applied. Figure 25 shows the current in the odd harmonic components of each coil with and without series inductors, when conducting a 30 W class WPT experiment. As in the simulation, the current of the odd harmonic component when the series inductance was applied was reduced by a minimum of 35% to a maximum of 73% compared to when the series inductance was not applied.

Table 14. Measurement results of the Tx and Rx fundamental current components when operating a 30 W class WPT according to the presence of Ladd (30 μH).

Parameters	WO L_{add}	With L_{add} (30 μH)
Input fundamental current (I_1)	4.05 A_{peak}	4.27 A_{peak}
Output fundamental current (I_2)	3.48 A_{peak}	3.50 A_{peak}

(**a**)　　　　　　　　　　　　　　　　　(**b**)
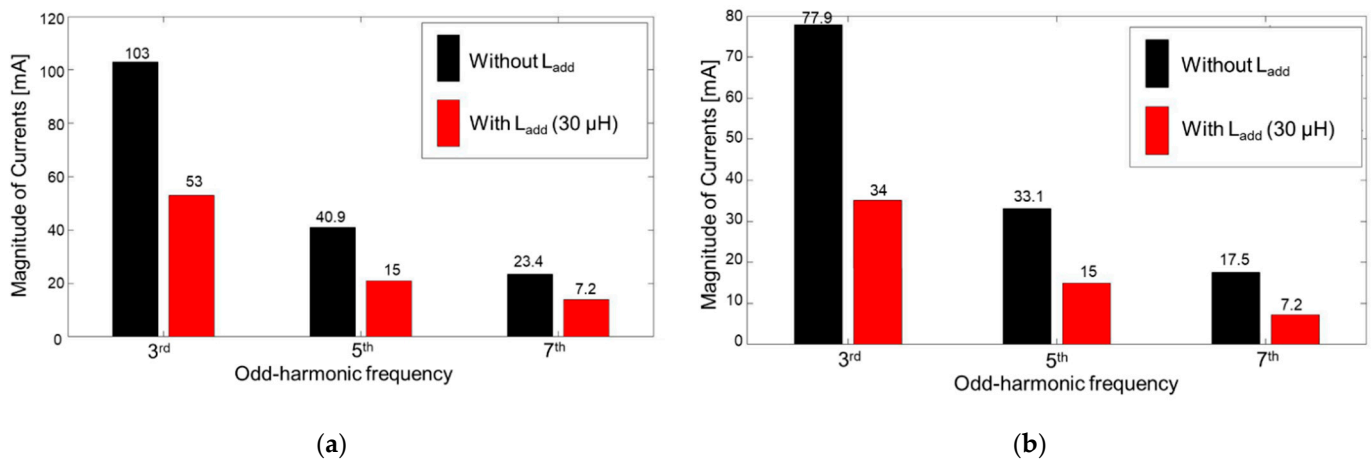
Figure 25. Measurement of the FFT of Tx and Rx current waveforms when operating a 30 W class WPT according to the presence of Ladd (30 μH): (**a**) comparison of odd harmonic components of Tx current (I_1); (**b**) comparison of odd harmonic components of Rx current (I_2).

Finally, the EMI was measured at a distance of 3 m in accordance with CISPR 14-1 standard [30], while the 30 W class WPT system was operating. Figure 26 shows the measurement setup. Table 15 shows the measured EMI data of the WPT system, and when the series inductance was applied. When the series inductance was applied, it reduced from 3.42 dBμA/m to a maximum of 9.02 dBμA/m compared to when it was not applied.
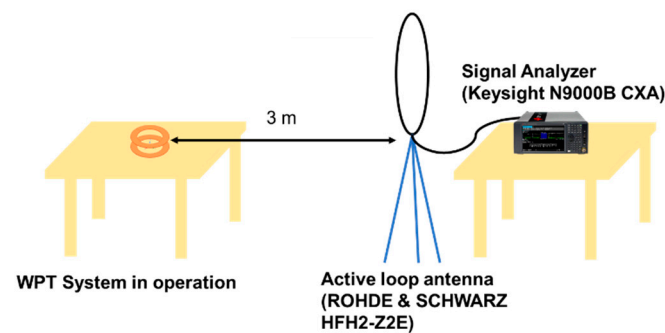
Figure 26. Equipment setup for measuring the EMI of the WPT system.

Table 15. Comparison of EMI results for WPT systems with and without series inductors (30 µH).

Frequency	Measured EMI		EMI Reduction [dBµA/m]
	WO L_{add} [dBµA/m]	With L_{add} (30 µH) [dBµA/m]	
Fundamental	17.05	22.21	+4.6
3rd harmonic	1.46	−7.56	−9.02
5th harmonic	−11.32	−15.97	−4.65
7th harmonic	−18.39	−21.81	−3.42

Meanwhile, Table A5 of Appendix D shows the standard of radiation emission defined in CISPR 14-1. Comparing the EMI measurement results of Table 15 with the EMI limit specifications of Table A5, it can be seen that all measurement results, whether the series inductor is added or not, do not exceed the limit specifications. This is because the power transfer capacity is relatively low (30 W class), and if the power transfer capacity is increased, the measured EMI results may exceed the limit standard. Although there is a difference between the limit standard and the measured EMI values, it can be said that the WPT design with the additional series inductors has proved sufficiently effective because it effectively reduced EMI (maximum −9.02 dBµA/m).

5. Discussion

In this paper, we proved the contents analyzed by equations in the analysis through a system with resonance frequency of 60 kHz. The reason why a system with a resonant frequency of 60 kHz can be representative in the verification process is that the characteristics of an over-coupled WPT system and a WPT system with series inductors analyzed in the paper do not depend on resonance frequency. By looking at Equation (17) representing the PTE, Equation (18) representing the transferred power, Equation (24) representing the magnitude of the input impedance, and Equations (29) and (30) representing the current component of the coil, it can be seen that even if the resonant frequency changes, the analyzed characteristics do not change.

Figure 27 shows the analysis of the input impedance in the case of a WPT system with a resonance frequency of 100 kHz. While the WPT system analyzed in the paper has a resonant frequency of 60 kHz, the resonant frequency in Figure 27 is 100 kHz. Except that the natural resonance frequency (ω_1) has been shifted from 60 kHz to 100 kHz, all characteristics are identical. That is, it can be seen in Figure 27a that the slope of the input impedance increases in proportion to the added series inductance, and as the series inductance increases, the other two points of ZPA (ω_2, ω_3) converge to the natural resonance frequency (ω_1). Therefore, it can be inferred that the input impedance and series inductors of the over-coupled WPT system analyzed in this paper can be applied regardless of the resonance frequency.
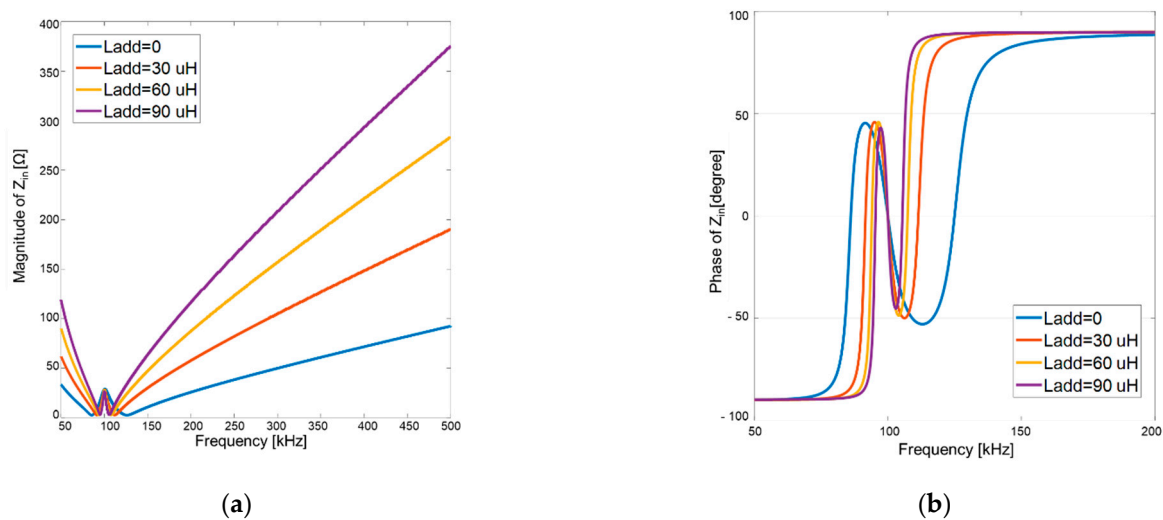
(**a**)

(**b**)

Figure 27. Input impedance change according to the series inductance value (L_{add-tx}, L_{add-rx}) when resonance frequency is 100 kHz: (**a**) input impedance magnitude change according to frequency change; (**b**) input impedance phase change according to frequency change.

6. Conclusions

In this paper, two problems of the over-coupled WPT system were analyzed. First, the over-coupled WPT system had a problem in that the slope of the input impedance in the harmonics was reduced, and the EMI issue in the harmonics component worsened. It was analyzed mathematically. In addition, another problem was analyzed—that the over-coupled WPT system has a limitation in that the frequency of the MPT and the frequency of the maximum PTE are different. This means that the MPT and maximum PTE values, which are very important in the WPT system, cannot be achieved simultaneously at operating frequency.

In order to solve the problems of the over-coupled WPT system, design considerations of the WPT system with series inductors were proposed. When series inductors are added to the WPT system, the slope of the input impedance in the harmonic component increases in proportion to the additional series inductance. It was found that the increase in the input impedance slope in harmonics has the effect of relatively increasing the input impedance, and the EMI issue is improved by reducing the current of the harmonic component of the WPT system with series inductors. Another problem of the over-coupled WPT system, the problem that the frequency of the MPT and the frequency of the maximum PTE is different, was also proven to be improved by applying series inductors.

The analysis was verified through simulation and experiment, and EMI was measured in a 30 W class WPT system with series inductors. The WPT system with added series inductors designed in consideration of the proposed contents of this paper has proven its effectiveness by obtaining a maximum EMI reduction of 9.02 dBµA/m with a 2% reduction in power transfer efficiency.

In the WPT system with series inductors analyzed in this paper, the efficiency decreases due to the parasitic resistance of the series inductance, but the relatively simple structure has the effect of reducing EMI, and the maximum PTE frequency and the MPT frequency become closer. Consequently, the proposed system has a total of two advantages. This simple structure has a certain advantage over other EMI reduction methods (reactive shield, active shield [15]) of the WPT system, and has the advantage that its versatility is very high as analyzed in this paper.

Appendix A

Figure A1 shows a typical circular coil. The coil has n turns. The magnetic field calculated at an arbitrary measurement point is as shown in Equations (A1)–(A3) [24].

$$|\vec{\mathbf{B}}| = \sqrt{B_x^2 + B_r^2} \tag{A1}$$

$$B_x = \frac{nI\mu_0}{2a\pi\sqrt{Q}}\left\{E(k)\frac{1 - \alpha^2 - \beta^2}{Q - 4\alpha} + K(k)\right\} \tag{A2}$$

$$B_r = \frac{nI\mu_0\gamma}{2a\pi\sqrt{Q}}\left\{E(k)\frac{1 + \alpha^2 + \beta^2}{Q - 4\alpha} - K(k)\right\} \tag{A3}$$
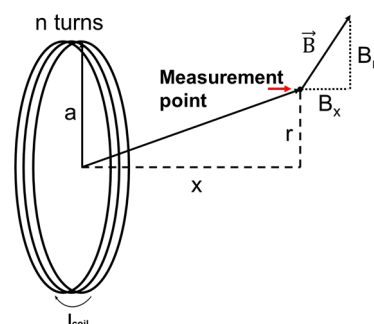

Figure A1. Magnetic field produced by a circular coil.

The detailed meaning of each character in Equations (A1)–(A3) is specified in Table A1 [24].

Table A1. Characters required for calculating the magnetic field of a circular coil.

Parameters	Value
α	$\frac{r}{a}$
β	$\frac{x}{a}$
γ	$\frac{x}{r}$
Q	$\left[\left(1 + \alpha\right)^2 + \beta^2\right]$
k	$\sqrt{\frac{4\alpha}{Q}}$
K(k)	$\int_0^{\frac{\pi}{2}} \frac{d\theta}{\sqrt{1 - k^2 \sin^2 \theta}}$
E(k)	$\int_0^{\frac{\pi}{2}} \sqrt{1 - k^2 \sin^2 \theta}\, d\theta$

K(k) is the complete elliptic integral of the first kind, and E(k) is the complete elliptic integral of the second kind [24].

Appendix B

Table A2. Simulation results of coil mutual inductance and coupling coefficient according to air gap.

Air Gap [mm]	Mutual Inductance [µH]	Coupling Coefficient
5	28.54	0.8
10	24.68	0.69
15	21.56	0.6
20	18.8	0.51
30	13.4	0.37
40	10.8	0.30
50	8.9	0.25
60	7.32	0.21
70	6.09	0.17
80	5.11	0.14
90	4.3	0.12
100	3.65	0.10

Appendix C

Table A3. Specifications of the toroidal core used to make the inductor.

Parameters	Value	
Toroidal core model	OR330H060	
Outer diameter	33.83 mm	data
Inner diameter	19.3 mm	
Height	11.61 mm	
Cross section	0.672 cm^2	
Path length	8.15 cm^2	
Window area	2.93 cm^2	
Permeability	60 µ	
AL value	61 [nH/N^2]	

Table A4. Results for the toroidal inductors as analyzed by EM solver [1].

Inductance [μH]	Number of Turns [turns]	Resistance [mΩ]
10	13	29
20	18	41
30	22	50
40	26	57
50	28	65
60	31	80
70	34	111
80	36	171
90	38	248

[1] Wire diameters used in all inductors are all equal to 1.0 mm.

Appendix D

Table A5. CISPR 14-1 Standard (EMC-Requirements for household appliances, electric tools and similar apparatus, Part 1: Emission) [30].

Frequency Range [MHz]	Limits at 3m Distance [dBμA/m]
0.009 to 0.070	69
0.070 to 0.150	Decreasing linearly with logarithm of frequency from 69 to 39
0.150 to 4.0	Decreasing linearly with logarithm of frequency from 39 to 3
4.0 to 30	3

References

1. Kim, D.; Jeong, D.; Kim, H.; Kim, J.; Park, S.-M.; Ahn, S. Design and Implementation of a Wireless Charging-Based Cardiac Monitoring System Focused on Temperature Reduction and Robust Power Transfer Efficiency. *Energies* **2020**, *13*, 1008. [CrossRef]
2. Kim, D.; Kim, H.; Huang, A.; He, Q.; Zhang, H.; Ahn, S.; Zhu, Y.; Fan, J. Analysis and Introduction of Effective Permeability with Additional Air-Gaps on Wireless Power Transfer Coils for Electric Vehicle Based on SAE J2954 Recommended Practice. *Energies* **2019**, *12*, 4797. [CrossRef]
3. Shin, J.; Shin, S.; Kim, Y.; Ahn, S.; Lee, S. Design and Implementation of Shaped Magnetic-Resonance-Based Wireless Power Transfer System for Roadway-Powered Moving Electric Vehicles. *IEEE Trans. Ind. Electron.* **2014**, *61*, 1179–1192. [CrossRef]
4. Tran, N.; Amri, M.; Park, J.H.; Hwang, S.; Kim, D.; Choi, K. A Novel Coding Metasurface for Wireless Power Transfer Applications. *Energies* **2019**, *12*, 4488. [CrossRef]
5. Choi, B.; Lee, E.; Sohn, Y.; Jang, G.; Rim, C. Six Degrees of Freedom Mobile Inductive Power Transfer by Crossed Dipole Tx and Rx Coils. *IEEE Trans. Power Electron.* **2015**, *31*, 3252–3272. [CrossRef]
6. Hui, S.Y. Planar Wireless Charging Technology for Portable Electronic Products and Qi. *Proc. IEEE* **2013**, *101*, 1290–1301. [CrossRef]
7. Hwang, K.; Cho, J.; Kim, D.; Park, J.; Kwon, J.H.; Kwak, S.I.; Park, H.; Ahn, S. An Autonomous Coil Alignment System for the Dynamic Wireless Charging of Electric Vehicles to Minimize Lateral Misalignment. *Energies* **2017**, *10*, 315. [CrossRef]
8. Lee, C.; Jung, G.; Al Hosani, K.; Song, B.; Seo, D.; Cho, D. Wireless Power Transfer System for an Autonomous Electric Vehicle. In Proceedings of the 2020 IEEE Wireless Power Transfer Conference (WPTC), Seoul, Korea, 15–18 November 2020; pp. 467–470.
9. Park, C.; Park, J.; Shin, Y.; Kim, J.; Huh, S.; Park, S.; Ahn, S. Separated Circular Capacitive Coupler for Reducing Cross-Coupling Capacitance in Drone Wireless Power Transfer System. *IEEE Trans. Microw. Theory Tech.* **2020**, *68*, 3978–3985. [CrossRef]
10. Huang, S.; Lee, T.; Li, W.-H.; Chen, R. Modular On-Road AGV Wireless Charging Systems via Interoperable Power Adjustment. *IEEE Trans. Ind. Electron.* **2019**, *66*, 5918–5928. [CrossRef]
11. Park, J.; Shin, Y.; Kim, D.; Park, B.; Ahn, S. Planar Resonance Reactive Shield for Reducing the EMI in Portable WPT Device Application. In Proceedings of the 2018 IEEE Symposium on Electromagnetic Compatibility, Signal Integrity and Power Integrity (EMC, SI & PI), Long Beach, CA, USA, 30 July–3 August 2018; pp. 419–422.
12. Campi, T.; Cruciani, S.; De Santis, V.; Maradei, F.; Feliziani, M. Near Field Wireless Powering of Deep Medical Implants. *Energies* **2019**, *12*, 2720. [CrossRef]
13. Christ, A.; Douglas, M.; Nadakuduti, J.; Kuster, N. Assessing Human Exposure to Electromagnetic Fields from Wireless Power Transmission Systems. *Proc. IEEE* **2013**, *101*, 1482–1493. [CrossRef]
14. Kim, H.; Song, C.; Kim, D.-H.; Jung, D.H.; Kim, I.; Ahn, S. Coil Design and Measurements of Automotive Magnetic Resonant Wireless Charging System for High-Efficiency and Low Magnetic Field Leakage. *IEEE Trans. Microw. Theory Tech.* **2016**, *64*, 383–400. [CrossRef]
15. Park, J.; Kim, D.; Hwang, K.; Park, H.H.; Kwak, S.I.; Kwon, J.H.; Ahn, S. A Resonant Reactive Shielding for Planar Wireless Power Transfer System in Smartphone Application. *IEEE Trans. Electromagn. Compat.* **2017**, *59*, 695–703. [CrossRef]

16. Cruciani, S.; Campi, T.; Maradei, F.; Feliziani, M. Active Shielding Design for a Dynamic Wireless Power Transfer System. In Proceedings of the 2020 International Symposium on Electromagnetic Compatibility—EMC EUROPE, Rome, Italy, 7–11 September 2020; pp. 1–4.

17. Wang, J.; Li, J.; Ho, S.L.; Fu, W.; Li, Y.; Yu, H.; Sun, M. Lateral and Angular Misalignments Analysis of a New PCB Circular Spiral Resonant Wireless Charger. *IEEE Trans. Magn.* **2012**, *48*, 4522–4525. [CrossRef]

18. Niu, W.-Q.; Chu, J.-X.; Gu, W.; Shen, A.-D. Exact Analysis of Frequency Splitting Phenomena of Contactless Power Transfer Systems. *IEEE Trans. Circuits Syst. I Regul. Pap.* **2012**, *60*, 1670–1677. [CrossRef]

19. Huang, R.; Zhang, B.; Qiu, D.; Zhang, Y. Frequency Splitting Phenomena of Magnetic Resonant Coupling Wireless Power Transfer. *IEEE Trans. Magn.* **2014**, *50*, 1–4. [CrossRef]

20. Xu, D.; Yin, S.; Wang, D. Analysis of frequency splitting phenomena for magnetic resonance wireless power transfer systems. In Proceedings of the 2017 Chinese Automation Congress (CAC), Jinan, China, 20–22 October 2017; pp. 2614–2618.

21. Steigerwald, R. A comparison of half-bridge resonant converter topologies. *IEEE Trans. Power Electron.* **1988**, *3*, 174–182. [CrossRef]

22. Kim, N.Y.; Kim, K.Y.; Ryu, Y.; Choi, J.; Yoon, C. Automated Adaptive Frequency Tracking System for Efficient Mid-Range Wireless Power Transfer via Magnetic Resonance Coupling. In Proceedings of the 42nd European Microwave Conference, Amsterdam, The Netherlands, 29 October–1 November 2012; pp. 221–224.

23. Chen, C.; Chu, T.-H.; Lin, C.; Jou, Z. A Study of Loosely Coupled Coils for Wireless Power Transfer. *IEEE Trans. Circuits Syst. II Express Briefs* **2010**, *57*, 536–540. [CrossRef]

24. Datta, S. Electric and Magnetic Fields from a Circular Coil Using Elliptic Integrals. *Phys. Educ.* **2007**, *2007*, 203–2012.

25. Ott, H.W. *Electromagnetic Compatibility Engineering*, 1st ed.; John Wiley & Sons: Hoboken, NJ, USA, 2009; pp. 174–178.

26. Song, C.; Kim, H.; Jung, D.H.; Kim, J.J.; Kong, S.; Kim, J.; Ahn, S.; Kim, J.; Kim, J. Low EMF and EMI Design of a Tightly Coupled Handheld Resonant Magnetic Field (HH-RMF) Charger for Automotive Battery Charging. *IEEE Trans. Electromagn. Compat.* **2016**, *58*, 1194–1206. [CrossRef]

27. Macrelli, E.; Romani, A.; Wang, N.; Roy, S.; Hayes, M.; Paganelli, R.P.; Mathuna, C.; Tartagni, M. Modeling, Design, and Fabrication of High-Inductance Bond Wire Microtransformers With Toroidal Ferrite Core. *IEEE Trans. Power Electron.* **2014**, *30*, 5724–5737. [CrossRef]

28. Eroglu, A. Complete Modeling of Toroidal Inductors for High Power RF Applications. *IEEE Trans. Magn.* **2012**, *48*, 4526–4529. [CrossRef]

29. Orlandi, S.; Blanchot, G.; Buso, S.; Faccio, F.; Fuentes, C.A.; Kayal, M.; Michelis, S.; Spiazzi, G. Optimization of Shielded PCB Air-Core Toroids for High-Efficiency DC–DC Converters. *IEEE Trans. Power Electron.* **2011**, *26*, 1837–1846. [CrossRef]

30. CISPR14-1. *Electromagnetic Compatibility—Requirements for Household Appliances, Electric Tools and Similar Apparatus Part 1: Emission*; International Electrotechnical Commission: Geneva, Switzerland, 2009.